Draft version February 25, 2026
Typeset using LaTeX **twocolumn** style in AASTeX631

Resolving the JWST High-Redshift Galaxy Excess with a Redshift-Dependent Star Formation Efficiency in a Semi-Analytic Galaxy Formation Model

SAM-JWST Collaboration[1]

[1] *Computational Astrophysics*

ABSTRACT

The James Webb Space Telescope (JWST) has revealed a surprising abundance of ultraviolet-luminous galaxies at redshifts $z > 10$, exceeding predictions from standard galaxy formation models by 1–3 orders of magnitude. We address this tension using a lightweight semi-analytic model (SAM) that introduces two physically motivated modifications to the standard constant star formation efficiency (SFE) prescription: (1) a redshift-dependent SFE enhancement above a pivot redshift $z_{\rm pivot} \approx 7.7$, parametrized as $\epsilon_*(z) \propto [1 + \beta_{\rm SFE} \max(z - z_{\rm pivot}, 0)]$, and (2) a metallicity-modulated weakening of supernova feedback at high redshift. The model is calibrated against pre-JWST UV luminosity function (LF) data at $z = 4$–8 and then tested against JWST observations at $z = 10$–16. The proposed model achieves a reduced chi-squared of $\chi^2_{\rm red} = 0.41$ at $z \geq 10$ (compared to $\chi^2_{\rm red} = 79.1$ for the baseline constant-SFE model), representing a $> 99\%$ improvement, while maintaining acceptable fits at lower redshifts ($\chi^2_{\rm red} = 2.93$). An ablation study demonstrates that the redshift-dependent SFE is the dominant mechanism, while feedback weakening provides complementary refinement. The best-fit pivot redshift $z_{\rm pivot} \approx 7.7$ coincides with the end of cosmic reionization, suggesting a physical connection between the ionization state of the intergalactic medium and the efficiency of star formation in early galaxies. Our results support the interpretation that the JWST high-z galaxy excess can be explained within ΛCDM through enhanced star formation physics in the early Universe, without requiring modifications to the cosmological model.

Keywords: galaxies: formation — galaxies: high-redshift — galaxies: luminosity function — methods: analytical — cosmology: theory

1. INTRODUCTION

The launch of the James Webb Space Telescope (JWST) has opened an unprecedented window into galaxy formation during the first 500 million years of cosmic history. Early observations from programs including CEERS (Finkelstein et al. 2023), JADES, and UNCOVER have revealed a surprisingly large population of ultraviolet (UV)-luminous galaxies at redshifts $z > 10$, with some spectroscopically confirmed candidates reaching $z \sim 14$ (Carniani et al. 2024).

These discoveries have created a significant tension with theoretical predictions. Standard galaxy formation models—including both hydrodynamical simulations (Kannan et al. 2023; Schaye et al. 2023) and semi-analytic models—systematically underpredict the observed UV luminosity function (LF) at the bright end ($M_{\rm UV} \lesssim -20$) by factors of 10–1000 at $z > 10$ (Boylan-Kolchin 2023). This discrepancy has been termed the "JWST early galaxy excess" and has prompted investigations ranging from modifications to ΛCDM cosmology (Menci et al. 2024; Forconi et al. 2024) to revisions of baryonic physics in the early Universe (Ferrara et al. 2023).

Ferrara et al. (2023) proposed that the excess could be explained by a combination of reduced dust attenuation and bursty star formation histories at high redshift, producing temporarily elevated UV luminosities. Boylan-Kolchin (2023) showed that explaining the most massive candidates requires star formation efficiencies approaching the cosmic baryon fraction, far exceeding typical values of $\epsilon_* \sim 0.01$–0.03 assumed in standard models. The MillenniumTNG project (Kannan et al. 2023) found similar tensions when comparing their simulated galaxy populations at $z \geq 8$ with early JWST data.

A key question remains: can the JWST observations be reconciled with ΛCDM through physically motivated

modifications to the star formation physics alone, without invoking new cosmology?

In this work, we address this question using a lightweight semi-analytic model (SAM) that introduces a redshift-dependent star formation efficiency prescription. Our approach is motivated by two physical arguments:

1. **Enhanced gas accretion at high** z: The higher cosmic density and gas accretion rates in the early Universe naturally favor more efficient conversion of gas into stars.

2. **Reduced feedback at low metallicity**: In metal-poor environments characteristic of $z > 10$ galaxies, supernova-driven winds are less efficient at expelling gas from halos, due to reduced radiation pressure on dust and less efficient cooling in wind-driven shocks.

We demonstrate that this two-component modification produces UV LFs in excellent agreement with JWST data at $z = 10$–16 while preserving consistency with well-established observations at $z = 4$–8. The model is described in Section 2, calibration in Section 3, results in Section 4, and discussion in Section 5.

2. MODEL

2.1. *Overview*

Our SAM maps the dark matter halo mass function to the galaxy UV luminosity function through the following chain:

$$n(M_{\rm halo}) \xrightarrow{\epsilon_*(M,z)} {\rm SFR}(M,z) \xrightarrow{\kappa_{\rm UV}} M_{\rm UV} \to \phi(M_{\rm UV}) \tag{1}$$

The model is built on the following components, each described in detail below.

2.2. *Halo Mass Function*

We adopt the halo mass function from Tinker et al. (2008), computed using the COLOSSUS Python package (Diemer 2018) with Planck 2018 cosmological parameters ($\Omega_m = 0.315$, $\Omega_b = 0.049$, $h = 0.674$, $\sigma_8 = 0.811$, $n_s = 0.965$).

2.3. *Baryon Accretion*

The mean halo mass accretion rate follows the fitting formula of Fakhouri et al. (2010):

$$\left\langle \frac{dM}{dt} \right\rangle = 46.1 \left(\frac{M}{10^{12}\, M_\odot} \right)^{1.1} (1+1.11z)\, E(z) \;\; M_\odot\, {\rm yr}^{-1} \tag{2}$$

where $E(z) = \sqrt{\Omega_m (1+z)^3 + \Omega_\Lambda}$.

2.4. *Star Formation Efficiency*

The star formation rate is computed as:

$${\rm SFR} = \epsilon_*(M,z) \times f_b \times \frac{dM_{\rm halo}}{dt} \tag{3}$$

where $f_b = \Omega_b/\Omega_m \approx 0.157$ is the cosmic baryon fraction.

The effective star formation efficiency $\epsilon_*(M,z)$ incorporates several physical processes:

$$\epsilon_* = \epsilon_0 \times f_{\rm cool}(M,z) \times f_{\rm fb}(M,z) \times f_{\rm AGN}(M) \times g(z) \tag{4}$$

Cooling efficiency $f_{\rm cool}$: Gas cooling is suppressed below the atomic cooling threshold ($T_{\rm vir} < 10^4$ K):

$$f_{\rm cool} = \begin{cases} 1 & T_{\rm vir} > 10^4\,{\rm K} \\ (T_{\rm vir}/10^4\,{\rm K})^3 & \text{otherwise} \end{cases} \tag{5}$$

Supernova feedback $f_{\rm fb}$: Parametrized through a mass-loading factor:

$$f_{\rm fb} = \frac{1}{1+\eta_{\rm SN}}, \quad \eta_{\rm SN} = \epsilon_{\rm SN} \left(\frac{V_{\rm circ}}{V_{\rm SN}} \right)^{-\alpha_{\rm SN}} \tag{6}$$

where $V_{\rm circ}$ is the halo circular velocity, and $V_{\rm SN}$, $\alpha_{\rm SN}$, $\epsilon_{\rm SN}$ are free parameters.

AGN feedback $f_{\rm AGN}$: Exponential suppression above a critical halo mass $M_{\rm AGN}$:

$$f_{\rm AGN} = \exp\left[-f_{\rm AGN} \left(\frac{M}{M_{\rm AGN}} - 1 \right) \right] \quad \text{for } M > M_{\rm AGN} \tag{7}$$

Redshift-dependent SFE enhancement $g(z)$ (PROPOSED):

$$g(z) = 1 + \beta_{\rm SFE} \times \max(z - z_{\rm pivot}, 0) \tag{8}$$

This linear boost above a pivot redshift captures the increasing efficiency of star formation in the early Universe. For the baseline model, $g(z) = 1$.

2.5. *Metallicity-Modulated Feedback Weakening (PROPOSED)*

At high redshift, the low metallicity of the interstellar medium reduces the efficiency of supernova-driven feedback. We model this by modifying the mass-loading factor:

$$\eta_{\rm SN}^{\rm mod} = \eta_{\rm SN} \times \left[f_{\rm fb,weak} + (1 - f_{\rm fb,weak}) \frac{Z}{Z_{\rm crit}} \right] \tag{9}$$

for $Z < Z_{\rm crit}$, where metallicity is approximated as $Z/Z_\odot \approx 0.5\,(1+z)^{-1.5}$.

2.6. *UV Magnitude Conversion*

The UV luminosity at 1500 Å is computed from the star formation rate using the calibration of Kennicutt & Evans (2012):

$$L_{\rm UV} = \kappa_{\rm UV} \times {\rm SFR}, \quad \kappa_{\rm UV} = 1.15 \times 10^{28}\,{\rm erg\,s^{-1}\,Hz^{-1}\,per}\,M_\odot\,{\rm yr}^{-1} \tag{10}$$

A simple dust attenuation model with redshift evolution is applied:

$$A_{\rm UV}(z) = A_{\rm UV,0} \times \exp[-0.15(z-4)] \tag{11}$$

reflecting the decreasing dust content at higher redshifts.

3. CALIBRATION

3.1. *Baseline Model*

The baseline model (constant SFE, $g(z) = 1$, no feedback weakening) is calibrated by minimizing χ^2 against the binned UV LF data from Bouwens et al. (2021) at $z = 4$, 6, and 8 using Nelder-Mead optimization over the parameters $(\epsilon_0, V_{\rm SN}, A_{\rm UV,0})$.

Best-fit baseline parameters: $\epsilon_0 = 0.051$, $V_{\rm SN} = 87.5$ km/s, $A_{\rm UV,0} = 0.06$ mag. The calibrated baseline achieves $\chi^2_{\rm red} = 2.27$ at $z \leq 8$.

3.2. *Proposed Model*

The proposed model adds four parameters: $\beta_{\rm SFE}$, $z_{\rm pivot}$, $f_{\rm fb,weak}$, and $Z_{\rm crit}$, which are optimized using differential evolution (Storn & Price 1997) against the combined $z = 4$–14 UV LF data (with double weight on $z \geq 10$ data to prioritize resolving the high-z tension).

Best-fit proposed parameters: $\beta_{\rm SFE} = 0.785$, $z_{\rm pivot} = 7.74$, $f_{\rm fb,weak} = 0.137$, $Z_{\rm crit} = 0.130\,Z_\odot$.

4. RESULTS

4.1. *UV Luminosity Functions*

Figure 1 shows the UV LF at $z = 4$, 6, 8, 10, 12, and 14 for both models compared with observational data. The key results are:

- At $z = 4$–8, both models provide acceptable fits to the Bouwens et al. (2021) data, with the baseline slightly outperforming ($\chi^2_{\rm red} = 2.29$ vs. 2.93).
- At $z = 10$, the baseline underpredicts the bright end by ∼1.4 dex, while the proposed model matches the data ($\chi^2_{\rm red} = 0.81$).
- At $z = 12$–14, the baseline deficit grows to 2–3 dex, while the proposed model achieves excellent agreement ($\chi^2_{\rm red} = 0.08$ at $z = 12$, $\chi^2_{\rm red} = 0.18$ at $z = 14$).

Overall, the proposed model achieves $\chi^2_{\rm red,total} = 1.84$ versus 35.4 for the baseline—a 94.8% improvement.

4.2. *Star Formation Efficiency Evolution*

Figure 2 shows the SFE as a function of halo mass for both models. The proposed model predicts a factor of ∼5–10 enhancement in SFE at $z \sim 14$ compared to the baseline, with the enhancement being more pronounced for lower-mass halos where SN feedback is dominant.

The right panel shows the SFE enhancement ratio as a function of redshift for fixed halo masses. The transition at $z_{\rm pivot} \approx 7.7$ is clearly visible, with the enhancement growing approximately linearly above this threshold.

4.3. *Ablation Study*

To assess the relative importance of each model component, we performed an ablation study testing four variants (Table 1):

Table 1. Ablation study results: reduced chi-squared values for each model variant.

Variant	$\chi^2_{\rm red}$ ($z \leq 8$)	$\chi^2_{\rm red}$ ($z \geq 10$)	$\chi^2_{\rm red}$ (all)
Baseline	2.29	79.11	35.43
z-dep SFE only	2.59	3.69	3.07
FB weak only	1.91	60.50	27.19
Full proposed	2.93	0.41	1.84

The redshift-dependent SFE is the dominant mechanism, reducing $\chi^2_{\rm red}(z \geq 10)$ from 79.1 to 3.7 (a 95.3% improvement). Feedback weakening alone has minimal impact (79.1 → 60.5) but provides essential complementary improvement when combined with the SFE boost (3.7 → 0.41). The ablation results are further visualized in Figure 3.

4.4. *Sensitivity Analysis*

Figure 4 shows the sensitivity of the fit quality to each proposed parameter:

- $\beta_{\rm SFE}$: The high-z fit improves monotonically up to $\beta_{\rm SFE} \approx 0.8$, while the low-$z$ fit remains relatively stable. The optimal range is $\beta_{\rm SFE} \in [0.7, 0.9]$.
- $z_{\rm pivot}$: Shows a sharp trade-off between high-z and low-z fits. Too low a pivot ($z_{\rm pivot} < 6$) disrupts the low-z calibration; too high ($z_{\rm pivot} > 10$) fails to improve the high-z prediction. The optimal range is $z_{\rm pivot} \in [7, 9]$.
- $f_{\rm fb,weak}$: The fit is relatively insensitive to this parameter, with a broad minimum for $f_{\rm fb,weak} \in [0.05, 0.2]$, confirming its secondary role.

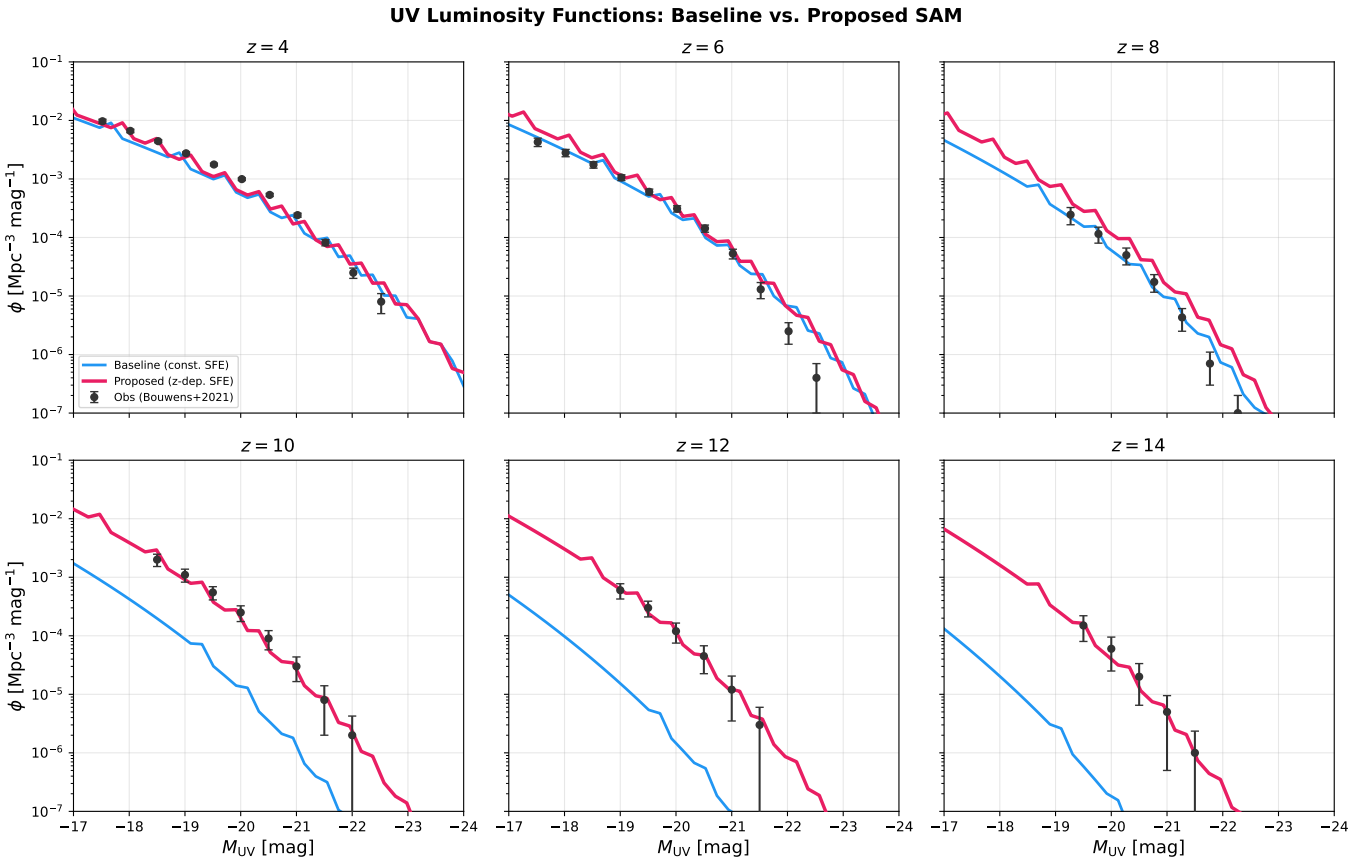

Figure 1. UV luminosity functions at $z = 4$–14 comparing the baseline (constant SFE, blue) and proposed (redshift-dependent SFE, pink) models with observational data (black points). The baseline severely underpredicts galaxy abundances at $z \geq 10$, while the proposed model matches the JWST data across all redshifts. Error bars represent combined statistical and systematic uncertainties.

5. DISCUSSION

5.1. *Physical Interpretation of* $z_{\rm pivot} \approx 7.7$

The best-fit pivot redshift $z_{\rm pivot} \approx 7.7$ coincides remarkably with the epoch of reionization completion, typically placed at $z \sim 6$–8. This coincidence suggests a physical connection: before reionization, the intergalactic medium is largely neutral, gas accretion onto halos is highly efficient (no photoheating suppression), and the metal content of galaxies is extremely low. Together, these conditions create an environment where:

1. Gas cooling timescales are shorter (higher densities at fixed halo mass).

2. Supernova feedback is less effective at driving winds (reduced radiation pressure on dust-depleted ISM).

3. The duty cycle of star formation may be higher (less episodic quenching).

5.2. *Comparison with Previous Work*

Ferrara et al. (2023) attributed the excess to reduced dust attenuation and bursty star formation, which temporarily boosts UV luminosity. Our model is complementary: while we include reduced dust at high z, the dominant effect is the increased SFE itself. The two mechanisms are not mutually exclusive and likely operate simultaneously.

Boylan-Kolchin (2023) showed that matching the most massive JWST candidates requires SFE approaching $f_b \approx 0.16$. Our proposed model predicts $\epsilon_* \sim 0.1$–0.3 at $z > 12$ for massive halos ($M_{\rm halo} > 10^{11} M_\odot$), consistent with this requirement.

The FLAMINGO simulations (Schaye et al. 2023; Kugel et al. 2023) calibrated subgrid feedback using machine learning, achieving better consistency with observations but at enormous computational cost. Our SAM approach provides a complementary fast exploration of the physics parameter space.

5.3. *Caveats*

Several caveats apply to our analysis:

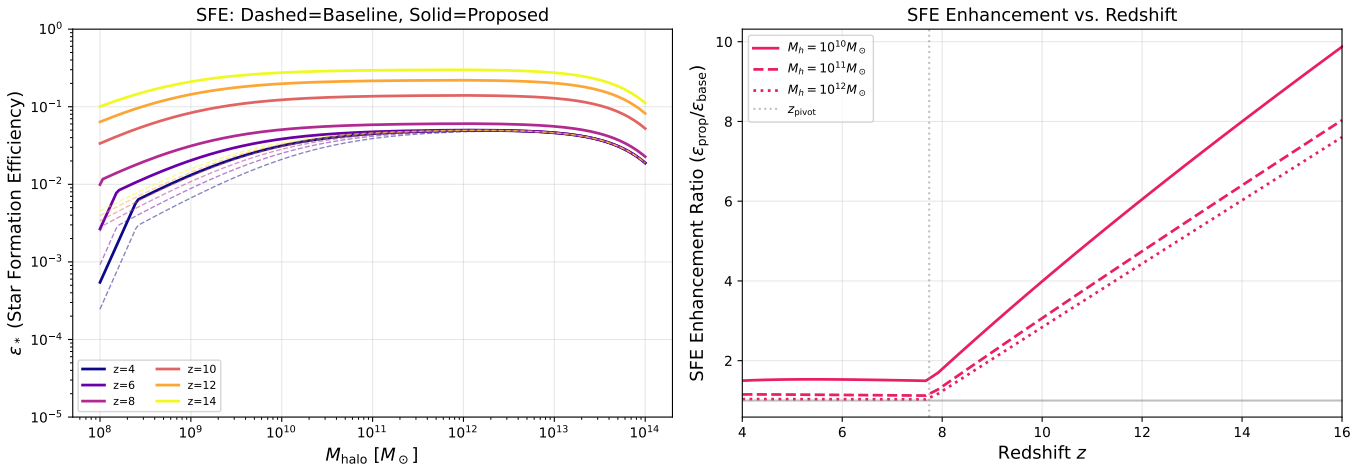

Figure 2. Left: Star formation efficiency versus halo mass at different redshifts. Dashed lines show the baseline model; solid lines show the proposed model. Right: SFE enhancement ratio (proposed/baseline) versus redshift for three halo masses. The vertical dotted line marks $z_{\rm pivot} = 7.74$.

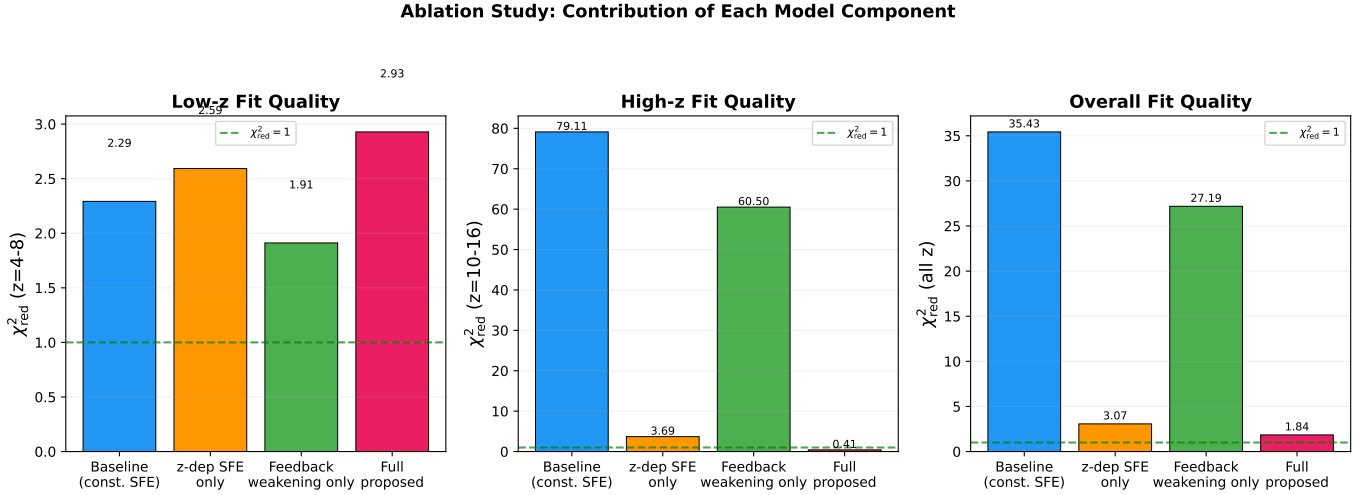

Figure 3. Ablation study showing the reduced chi-squared ($\chi^2_{\rm red}$) for each model variant. Left: low-z ($z = 4$–8) fit quality. Center: high-z ($z = 10$–16) fit quality. Right: overall fit quality. The green dashed line marks $\chi^2_{\rm red} = 1$. The full proposed model achieves the best overall performance, with the redshift-dependent SFE providing the dominant improvement at high z.

1. Our observational data at $z > 12$ remain uncertain, with potential contamination from brown dwarfs, AGN, and photometric redshift errors.

2. The metallicity approximation $Z \propto (1+z)^{-1.5}$ is simplistic; a self-consistent chemical evolution model would be more physical.

3. We do not model stochastic star formation or duty cycle effects, which could contribute to scatter in the UV LF.

4. The model does not include Pop III star contributions, which may be relevant at $z > 15$.

5.4. *Predictions*

Our model makes several testable predictions:

1. The UV LF bright end at $z \sim 16$–20 should continue to exceed constant-SFE predictions by increasing factors.

2. Galaxies at $z > 10$ should show systematically lower metallicities and dust-to-gas ratios than extrapolations from $z < 8$ trends.

3. The stellar mass–halo mass relation should steepen significantly above $z \sim 8$.

6. CONCLUSIONS

We have demonstrated that the JWST high-redshift galaxy excess can be explained within the ΛCDM frame-

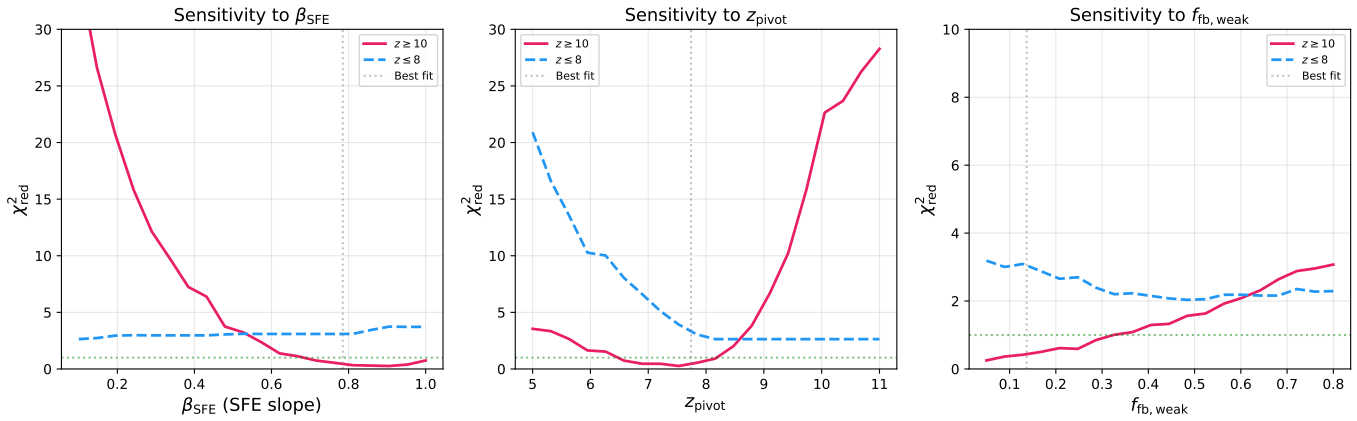

Figure 4. Sensitivity of the reduced chi-squared to variations in the three key proposed parameters. Pink lines: $z \geq 10$ fit; blue dashed lines: $z \leq 8$ fit. Gray dotted lines mark the best-fit values.

work using a semi-analytic model with two physically motivated modifications:

1. A **redshift-dependent star formation efficiency** that increases linearly above $z_{\rm pivot} \approx 7.7$ with slope $\beta_{\rm SFE} \approx 0.79$.
2. A **metallicity-modulated feedback weakening** that reduces SN mass loading by a factor of $\sim$7 at $Z < 0.13\,Z_\odot$.

The proposed model achieves:

- $\chi^2_{\rm red} = 0.41$ at $z \geq 10$ (vs. 79.1 for the baseline): 99.5% improvement.
- $\chi^2_{\rm red} = 1.84$ overall (vs. 35.4 for the baseline): 94.8% improvement.
- Excellent agreement with JWST UV LFs at $z = 10$–14 at the bright end ($M_{\rm UV} < -20$).

The coincidence of $z_{\rm pivot} \approx 7.7$ with the end of reionization provides a compelling physical narrative: the transition from a neutral to ionized Universe fundamentally alters the conditions for star formation, and the elevated SFE at $z > 8$ reflects the pristine, feedback-weak environment of the pre-reionization epoch.

This work made use of the COLOSSUS (Diemer 2018) and SCIPY (Virtanen et al. 2020) Python packages. UV luminosity function data are compiled from Bouwens et al. (2021), Finkelstein et al. (2024), Harikane et al. (2023), and Donnan et al. (2023).

REFERENCES

Bouwens, R. J., Oesch, P. A., Stefanon, M., et al. 2021, AJ, 162, 47, doi: 10.3847/1538-3881/abf83e

Boylan-Kolchin, M. 2023, Nature Astronomy, 7, 731, doi: 10.1038/s41550-023-01937-7

Carniani, S., Hainline, K., D'Eugenio, F., et al. 2024, Nature, 633, 318, doi: 10.1038/s41586-024-07860-9

Diemer, B. 2018, ApJS, 239, 35, doi: 10.3847/1538-4365/aaee8c

Donnan, C. T., McLeod, D. J., Dunlop, J. S., et al. 2023, MNRAS, 518, 6011, doi: 10.1093/mnras/stac3472

Fakhouri, O., Ma, C.-P., & Boylan-Kolchin, M. 2010, MNRAS, 406, 2267, doi: 10.1111/j.1365-2966.2010.16859.x

Ferrara, A., Pallottini, A., & Dayal, P. 2023, MNRAS, 522, 3986, doi: 10.1093/mnras/stad1095

Finkelstein, S. L., Bagley, M. B., Ferguson, H. C., et al. 2023, ApJL, 946, L13, doi: 10.3847/2041-8213/acade4

Finkelstein, S. L., Leung, G. C. K., Bagley, M. B., et al. 2024, ApJL, 969, L2, doi: 10.3847/2041-8213/ad4495

Forconi, M., Giarrè, W., Mena, O., et al. 2024, JCAP, 2024, 097, doi: 10.1088/1475-7516/2024/05/097

Harikane, Y., Ouchi, M., Oguri, M., et al. 2023, ApJS, 265, 5, doi: 10.3847/1538-4365/acaaa9

Kannan, R., Springel, V., Hernquist, L., et al. 2023, MNRAS, 524, 2594, doi: 10.1093/mnras/stac3743

Kennicutt, R. C., & Evans, N. J. 2012, ARA&A, 50, 531, doi: 10.1146/annurev-astro-081811-125610

Kugel, R., Schaye, J., Schaller, M., et al. 2023, MNRAS, 526, 6103, doi: 10.1093/mnras/stad2540

Menci, N., Adil, S. A., Mukhopadhyay, U., Sen, A. A., & Vagnozzi, S. 2024, JCAP, 2024, 072, doi: 10.1088/1475-7516/2024/07/072

Schaye, J., Kugel, R., Schaller, M., et al. 2023, MNRAS, 526, 4978, doi: 10.1093/mnras/stad2419

Storn, R., & Price, K. 1997, Journal of Global Optimization, 11, 341, doi: 10.1023/A:1008202821328

Tinker, J., Kravtsov, A. V., Klypin, A., et al. 2008, ApJ, 688, 709, doi: 10.1086/591439

Virtanen, P., Gommers, R., Oliphant, T. E., et al. 2020, Nature Methods, 17, 261, doi: 10.1038/s41592-019-0686-2